Journal of Photonics for Energy

PhotonicsforEnergy.SPIEDigitalLibrary.org

Investigation of low-bandgap nonfullerene acceptor-based polymer solar cells with very low photovoltage loss

Ying Zhang
Delong Liu
Patrick W. K. Fong
Gang Li

SPIE.

Ying Zhang, Delong Liu, Patrick W. K. Fong, Gang Li, "Investigation of low-bandgap nonfullerene acceptor-based polymer solar cells with very low photovoltage loss," *J. Photon. Energy* **9**(4), 045502 (2019), doi: 10.1117/1.JPE.9.045502.

Investigation of low-bandgap nonfullerene acceptor-based polymer solar cells with very low photovoltage loss

Ying Zhang,[a,b] Delong Liu,[b] Patrick W. K. Fong,[b] and Gang Li[a,b]
[a]Hong Kong Polytechnic University, Shenzhen Research Institute, Shenzhen, Guangdong, China
[b]Hong Kong Polytechnic University, Department of Electronic and Information Engineering, Hung Hom, Hong Kong, China

Abstract. Polymer solar cells (PSCs) have seen great progress in recent years, with power conversion efficiencies of over 15%. However, PSCs suffer from larger energy losses than inorganic and perovskite solar cells, leading to lower open-circuit voltage (V_{OC}). The main factors that hinder the V_{OC} improvements include (i) relatively large nonradiative recombination losses and thus low electroluminescence quantum efficiency (EQE_{EL}) in PSCs and (ii) the existence of a charge transfer state at the interface of donor and acceptor. For efficient charge separation in state-of-the-art PSCs, empirically, the driving force for exciton dissociation is considered to be at least 0.3 eV. The large driving force could lead to large voltage losses and thus hinder the PSC performance. In this study, we report using wide bandgap material PB3T as electron donor and low bandgap material IEICO-4F as electron acceptor for nonfullerene PSCs with very small driving forces, which, however, show a decent maximum external quantum efficiency (EQE) of nearly 40%. Moreover, we demonstrate a nonfullerene PSC with high EQE_{EL} up to 5.1×10^{-4}, corresponding to very low nonradiative recombination losses of 0.20 eV and overall photovoltage energy losses of 0.46 to 0.52 eV, derived from different bandgap (E_{gap}) determination methods, which can now be comparable to those in perovskite solar cells and inorganic solar cells. [DOI: 10.1117/1.JPE.9.045502]

Keywords: polymer solar cells; low bandgap acceptor; low photovoltage loss; nonradiative recombination loss.

Paper 19062 received Jun. 25, 2019; accepted for publication Oct. 18, 2019; published online Nov. 12, 2019.

1 Introduction

Polymer solar cells (PSCs) have attracted the interest of increasing numbers of researchers due to their great potential for fabricating flexible, light-weight, inexpensive, colorful, semitransparent, and large area devices.[1–3] Due to the rapid development of organic photovoltaic (PV) materials, a power conversion efficiency (PCE) of over 15%[4–6] for single-junction solar cells has recently been achieved. However, the device performances of the state-of-the-art PSCs still lag behind those of inorganic crystalline solar cells (silicon, GaAs, CdTe, etc.) and more recent perovskite solar cells. The foremost reason is that most of these PSCs suffer from substantial losses in open-circuit voltage (V_{OC}), which comes from the fundamental requirement of electron donor and acceptor materials in the bulk-heterojunction (BHJ)[7] and with energy level offsets for efficient Frenkel exciton dissociation.[8,9] Therefore, quantifying the voltage losses in different active layer material systems and investigating their variations with molecular structures have important implications for maximizing the device V_{OC} and reducing the difference between the theoretical and actual cases.

Electrically, a solar cell is typically modeled by a current generator in parallel with a diode. The V_{OC} is the voltage at the condition when the dark current (J_{dark}) in the diode and short-circuit photocurrent (J_{SC}) are equal, i.e., $J_{dark} = J_{SC}$. For an ideal diode, $J_{dark} = J_0(e^{\frac{qv}{kT}} - 1)$, and therefore, the V_{OC} can be given by the following expression: $V_{OC} = \frac{kT}{q}(\ln \frac{J_{SC}}{J_0} + 1)$, where k is the Boltzmann constant, T is the temperature in Kelvin, q is the elementary charge, and J_0 is a constant. Thus, we can use the reciprocity relation between PV EQE and electroluminescence (EL) spectra to quantify the V_{OC} reduction.[10] Using this

*Address all correspondence to Gang Li, E-mail: gang.w.li@polyu.edu.hk; Delong Liu, E-mail: delongl@iccas.ac.cn

1947-7988/2019/$28.00

method, recent studies have divided the voltage losses into three contributions from the Shockley–Queisser (SQ) limit point of view, i.e., $q\Delta V = q\Delta V_{OC}^{rad,SQ} + q\Delta V_{OC}^{rad,below\ gap} + q\Delta V_{OC}^{non\text{-}rad} = \Delta E_1 + \Delta E_2 + \Delta E_3$.[11,12] The first term $q\Delta V_{OC}^{rad,SQ}$ is universal for any solar cell, depends only on bandgap, and is due to blackbody radiative recombination. In BHJ PSC system, it is the lower bandgap component that determines this term.[13] The second term $q\Delta V_{OC}^{rad,below\ gap}$ comes from the charge transfer state (CTS) in D/A BHJ PSC, due to the requirement for exciton dissociation. It has been found that the ΔE_2 term can be minimized by lowering the energy offset between donor and acceptor molecular energy levels.[11,14–16] Moreover, the third term, $q\Delta V_{OC}^{non\text{-}rad}$, which has been considered as another main limiting problem for photovoltage loss in organic PV due to the lower level of ordering, can be quantified by the external quantum yield of EL with the equation of $q\Delta V_{OC}^{non\text{-}rad} = -kT\ \ln(EQE_{EL})$.[10] Although we can change the energy levels of the materials by molecular design for decreasing the second term in voltage loss, for the third term, the EQE_{EL} of blend film varies largely with different active layer material combination.[17] For example, when blending different polymeric donors PTB7-Th and PNOz4T with the identical electron acceptor phenyl-C71-butyric acid methyl ester ($PC_{71}BM$) to fabricate PSCs, the device based on PNOz4T:$PC_{71}BM$ exhibited an EQE_{EL} of 1.1×10^{-4} with a corresponding nonradiative recombination loss of 0.24 eV, whereas the EQE_{EL} in PTB7-Th:$PC_{71}BM$-based device decreased significantly to 8.6×10^{-8} with a nonradiative recombination loss of 0.42 eV.[14] Moreover, another study relating to voltage losses in nonfullerene PSCs comprising two perylene diimide-based small molecule acceptors in combination with four representative polymer donors found that both nonradiative recombination and radiative recombination losses are suppressed with decreasing energetic offsets between donor and acceptor materials, in addition to the variation of voltage losses of PV devices.[16] Similar phenomenon with low energetic offsets leading to a strong suppression in the nonradiative recombination voltage loss was also reported by Nelson's group recently; it was attributed to the hybridization between CT and lowest donor or acceptor exciton states, resulting in effective CT to ground state oscillator strength due to the intensity borrowing mechanism.[18] In addition, Nelson's group reported that the lower bandgap material in active layer blend has a high oscillator strength for transitions from the excited state to the ground state, i.e., enhancing the material luminescence is equally beneficial for decreasing the nonradiative recombination voltage loss.[18] In addition to investigating the sophisticated relationships among the above-said parameters, the question of how to increase the EQE_{EL} of PV device from the viewpoint of molecular design remains difficult to answer. Therefore, a careful analysis of voltage losses in different material systems is necessary and urgent for the further development of efficient organic PV materials.

In the fullerene acceptor era, the scientists worked hard to reduce the bandgap–qV_{OC} offset W_{OC}, defined by $E_{gap} - qV_{oc}$, or simply called photovoltage energy loss E_{loss}, from ~1.3 eV in P3HT:PCBM system[12] to ~0.8 eV in PTB series polymer:PCBM systems[12,14,19,20] and to ~0.7 eV (even lower than 0.6 eV) in low bandgap (LBG) polymer systems (Diketopyrrolopyrrole based, etc.).[12,21–24] The success of nonfullerene acceptors (NFAs) significantly shifts the paradigm of the PSC field, leading to significant progress in PSC efficiency, accompanied by lower V_{OC} loss. Among PSC systems, LBG organic PV materials have special significance, particularly in potential tandem solar cell development, as well as unique semitransparent solar cell applications.[25,26] In the past five years, small molecular NFAs have been seriously investigated due to their advantages of high flexibility in tuning electrochemical and optoelectronic properties via a relatively simple synthesis route.[4,27–29] IEICO-4F is an excellent representative ultra LBG NFA with absorption beyond 1000 nm and has been shown to have PSC efficiency of over 12% using classical PBT7-Th polymer as donor.[30] In this work, we aim to explore the limitation of the V_{OC} loss in IEICO-4F-based PSC system. We selected a wide-bandgap polymer PB3T as electron donor, which has a deeper highest occupied molecular orbital (HOMO) level than PTB7-Th, and IEICO-4F as electron acceptor to fabricate binary nonfullerene PSCs. This PSC material system has a very small HOMO energetic offset (~0.05 eV). The quantitative analysis of voltage losses was investigated based on classical SQ theory and the EQE_{EL}. The W_{OC} is found to be 0.46 to 0.52 eV, using different main-stream bandgap determination methods on the same system. The W_{OC} is the lowest achieved in IEICO-4F-based PSC and is among the lowest reported values in all PSCs reported. Specifically, with the thermodynamic SQ loss ΔE_1 of 0.24 eV, the EQE_{EL} of the system is found to

be high, which leads to record low PSC nonradiative recombination loss ΔE_3 of 0.20 eV, which is comparable to that of crystalline silicon solar cells or perovskite solar cells. The ΔE_2 is calculated to be only 0.02 to 0.08 eV and agrees well with the very small donor–acceptor HOMO offest; at the same time, the solar cell EQE is still significant at the level of ~40%.

2 Results and Discussion

2.1 *Material Structure and Basic Properties*

Figure 1(a) displays the chemical structures of the PB3T and IEICO-4F. The materials HOMO and lowest unoccupied molecular orbital estimated form the ionization potential (IP) and electron affinity (EA) are shown in Fig. 1(b).[29,31] From the cyclic voltammetry measurement, the IP and the EA are estimated to be −5.39 eV/ − 3.37 eV and −5.44 eV/ − 4.19 eV for PB3T and IEICO-4F, respectively. It can be found that the IP offset between PB3T and IEICO-4F is only about 0.05 eV, indicating a small driving force for exciton disassociation at the interfacial layer between PB3T and IEICO-4F. Figure 1(c) shows the normalized UV–vis absorption spectra of PB3T and IEICO-4F in films. The absorption region of PB3T falls in the range of 300 to 650 nm, whereas IEICO-4F has a significant red-shifted absorption region of 600 to 1000 nm due to the strong electron push–pull effect. The absorption edge of PB3T and IEICO-4F locates at 633 and 968 nm, respectively, corresponding to an optical bandgap of 1.96 and 1.28 eV.

2.2 *Photovoltaic Performances*

The sandwich-type PSCs were fabricated with a device structure of indium tin oxide (ITO)/PEDOT:PSS(poly(3,4-ethylenedioxythiophene):poly(styrene-sulfonate))/PB3T:IEICO-4F/poly[(9,9-bis(3-(*N*,*N*-dimethyl)-*N*-ethylammonium)-propyl)-2,7-fluorene)-alt-2,7-(9,9-dioctylfluorene)] dibromide (PFN-Br)/Ag, as shown in Fig. 2(a). PEDOT:PSS and PFN-Br were applied as interfacial layers for hole and electron transport, respectively. The device was tested under simulated AM 1.5G, 100 mW/cm^2 irradiance with an area of 0.08 cm^2. The PV performances of devices were optimized by different mass ratios of PB3T and IEICO-4F, solvent additive, and thermal annealing (TA), their corresponding *J*–*V* curves are shown in Figs. 6(a)–6(c) and EQE spectrum for devices with varied mass ratios are displayed in Fig. 6(d). The detailed PV data are summarized in Tables 4–7 for different donor/acceptor ratio, solvent additive and thermal

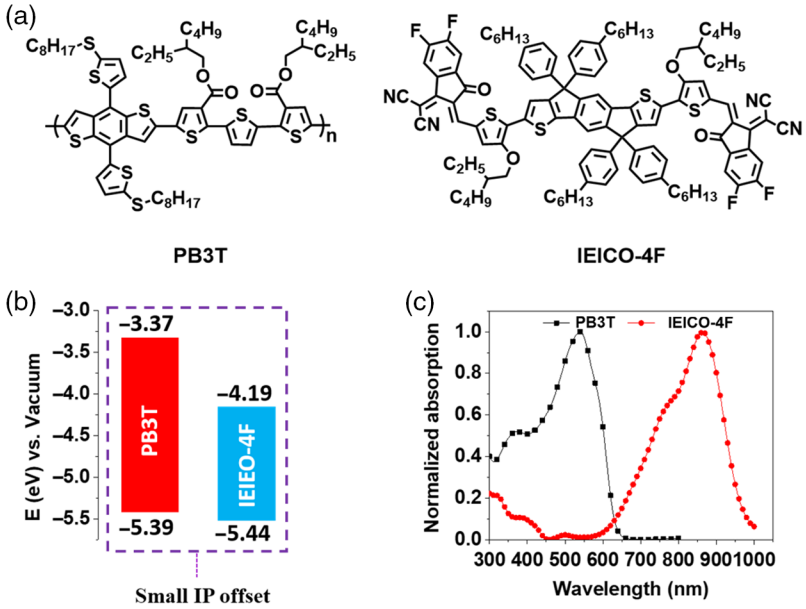

Fig. 1 (a) Chemical structures of the donor and acceptor, (b) energy level diagram, and (c) UV–Vis absorption spectra of PB3T and IEICO-4F in solid films.

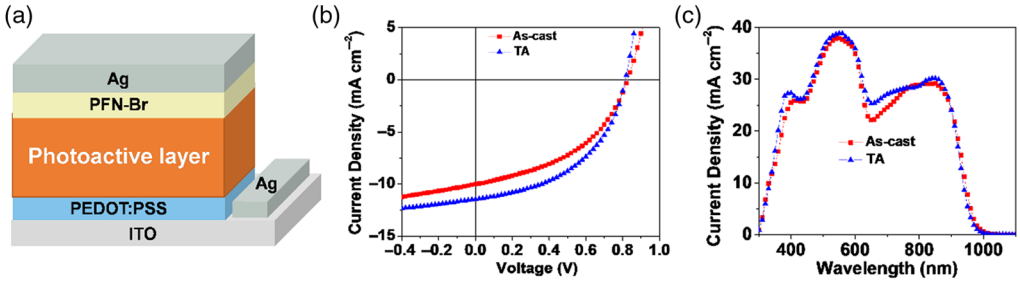

Fig. 2 (a) The conventional device structure used in this work. (b) The current density–voltage (J–V) curves and (c) EQE plot of the PB3T:IEICO-4F devices of as-cast and after TA.

Table 1 Detailed photovoltaic performances of the devices based on PB3T:IEICO-4F under standard AM 1.5 G illumination.

Devices	V_{OC} (V)	J_{SC} (mA/cm^2)	FF	PCE (%)	J_{calc}[a] (mA/cm^2)	EQE at λ_{max} (%)	E_{loss} (eV)
As-cast	0.82 (0.817 ± 0.008)	10.20 (10.09 ± 0.33)	0.44 (0.430.02)	3.68 (3.58 ± 0.22)	10.13	29.27	0.48
TA[b]	0.81 (0.805 ± 0.007)	11.47 (11.01 ± 0.34)	0.48 (0.47 ± 0.02)	4.46 (4.29 ± 0.10)	10.52	38.85	0.49

Note: The average photovoltaic parameters were calculated from 10 independent cells.
[a]The J_{calc} was calculated from the EQE spectrum.
[b]TA denotes thermal annealing at 130°C for 10 min.

annealing temperature and thermal annealing time, respectively. The as-cast device with a D:A weight ratio of 1:1.5 showed a PCE of 3.68% with a J_{SC} of 10.02 mA/cm^2, a V_{OC} of 0.82 V, and an FF of 0.44. After the optimization of TA at 130°C for 10 min, a champion PCE of 4.46% was obtained with a J_{SC} of 11.47 mA/cm^2, a V_{OC} of 0.81 V, and an FF of 0.48. The corresponding current–voltage (J–V) curves and PV parameters of as-cast and optimized devices optimization are displayed in Fig. 2(b) and Table 1. The EQE spectra of the as-cast and optimized devices are displayed in Fig. 2(c). The EQE response of all devices covers a wide range from 300 to 1000 nm, which is correlated with the absorption spectra of the blend film. The near-infrared absorption is from the absorption of the LBG acceptor IEICO-4F. After TA treatment, an improvement of photocurrent response was observed almost in all absorption regions, which is in accordance with the improvement of J_{SC}. Noticeably, the maximum EQE response of the best device of 38% was observed at ~550 nm, which is rarely found in previously reported organic solar cells with such a low HOMO difference.

2.3 *Charge Dissociation and Recombination*

To further study the photocurrent generation and exciton dissociation in this PSC system, the photocurrent density (J_{ph}) as a function of the effective voltage (V_{eff}) was examined, as is displayed in Fig. 3(a). Here, $J_{ph} = J_{light} - J_{dark}$, and J_{light} and J_{dark} refer to the current densities under illumination and dark conditions, respectively. $V_{eff} = V_0 - V_a$, where V_0 is the voltage when J_{light} equals J_{dark} ($J_{ph} = 0$), and V_a is the applied voltage. By applying high reverse bias, saturated photocurrent (J_{sat}) could be derived. It is clearly shown that the J_{ph} value of the best device saturated when V_{eff} reaches about 3 V, indicating that all generated excitons are separated under this condition. The dissociation efficiency [$P(E,T)$] of electron–hole pairs in the optimal device under short-circuit condition is examined by correcting J_{SC} as respect with J_{sat} (J_{ph}/J_{sat}). Noticeably, over 81% of photogenerated excitons dissociate into free carriers with smaller energy offset (<0.1 eV) based on the estimation of $J_{sat} = 13.3$ mA/cm^2. The $P(E,T)$ value in this system is comparable to those with highly efficient devices of around 90% or above.[28,32] Furthermore, the dependence of J_{SC} and V_{OC} on the various light intensities was examined to look insights into the charge recombination mechanism of the devices. The relationship of J_{SC} and light intensity can be expressed by a power-law equation of $J_{SC} \propto P_{light}^{\alpha}$, where

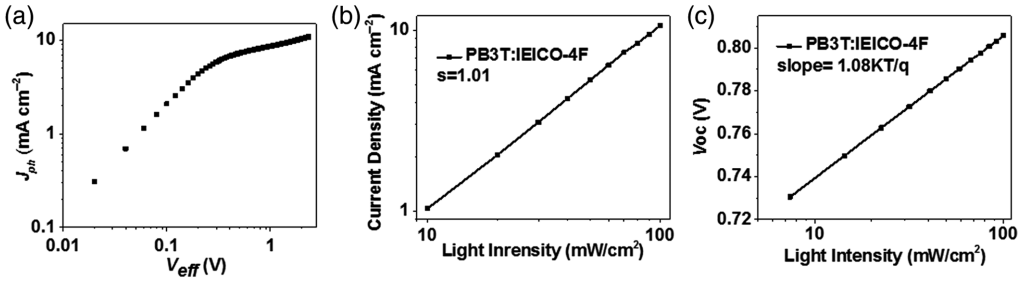

Fig. 3 (a) The photocurrent density (J_{ph}) versus the effective voltage (V_{eff}) for the optimized device, (b) the plot of J_{SC} versus light intensity, and (c) the plot of V_{OC} versus light intensity for the optimized device.

the power factor α is used to evaluate the degree of bimolecular recombination.[33] For a device with weak bimolecular recombination, α value is close to 1. In Fig. 3(b), curves are plotted on a log–log scale and the extracted slope value for the optimal device is close to unity, indicative of less bimolecular recombination in this D/A blended film. The dependence of V_{OC} on the light intensity could help study the main recombination mechanism at the V_{OC}, according to the equation of $V_{OC} \propto \frac{nkT}{q} \ln P_{light}$, where k_B is the Boltzmann constant, T is the temperature in Kelvin, and q is the elementary charge.[33] If bimolecular recombination dominants mechanism, the slope of n value versus the natural logarithm of the P_{light} should be k_BT/q. When a slope of $2k_BT/q$ is obtained, it becomes a trap-recombination-dominated device. In our cases, as is depicted in Fig. 3(c), the PB3T:IEICO-4F-based device exhibits a slope of $1.08k_BT/q$ at room temperature, revealing negligible trap-assisted recombination in this system. Hence, the PB3T:IEICO-4F-based devices show decent exciton dissociation efficiency and negligible trap-assisted recombination, even though they have a small driving force.

2.4 *Morphological Analysis*

We studied the morphological properties of the neat materials films and the PB3T:IEICO-4F blends films before and after TA treatments using tapping mode atomic force microscopy (AFM) and transmission electron microscopy (TEM). The neat PB3T and IEICO-4F show very smooth surfaces, and the root mean square (RMS) roughness of two films are 0.452 and 0.424 nm, respectively [see Figs. 8(a) and 8(b)]. As depicted in Figs. 4(a)–4(d), the blend film after TA process displays smoother surface (RMS = 1.69 nm) compared to the as-cast film (RMS = 1.74 nm). The AFM phase images of thermally annealed film show increased degree of phase separation with clear increased domain size, which may be prone to suppression of carrier recombination as well as improved FF for annealed solar cells. In the TEM images [Figs. 4(e) and 4(f)], a slightly more visible phase separation was observed in the blend film after TA.

2.5 *V_{OC} Loss Analysis*

As the total energy loss is determined by $E_{gap} - qV_{OC}$, the method used to determine E_{gap} affects a lot on the analysis of each part V_{OC} losses quantification. Here, the bandgap Egap was calculated by four mainstream methods based on (1) the derivative of EQE, (2) the Tauc plot, (3) the absorption edge, and (4) the crossover point of emission and absorption. Their corresponding E_{gap} values are 1.34 eV, 1.33 eV, 1.28 eV and 1.32 eV, respectively, estimated from curves in Figs. 17(a)–7(d). Table 2 made a list of the typical values of E_{loss} loss in terms of different E_{gap} definition by our methods. We found that the very small E_{loss} loss of about 0.46 to 0.52 eV can be obtained in PB3T/IEICO-4F system, which is comparable to those of inorganic solar cells and perovskite solar cells.[41] In addition, it is calculated ΔE_{HOMO} between donor and acceptor is 0.05 eV. Although this value is much lower than the empirical value of 0.3 eV,[42] commonly thought to be required for efficient exciton dissociation in fullerene system, it is still possible to get decent value of EQE_{max} close to 40%.

Based on the SQ limit mentioned above, the three terms of V_{OC} losses, i.e., ΔE_1, ΔE_2 and ΔE_3, were calculated. The first energy loss ΔE_1 (i.e., $q\Delta V_{OC}^{rad,SQ}$) is unavoidable in all types of

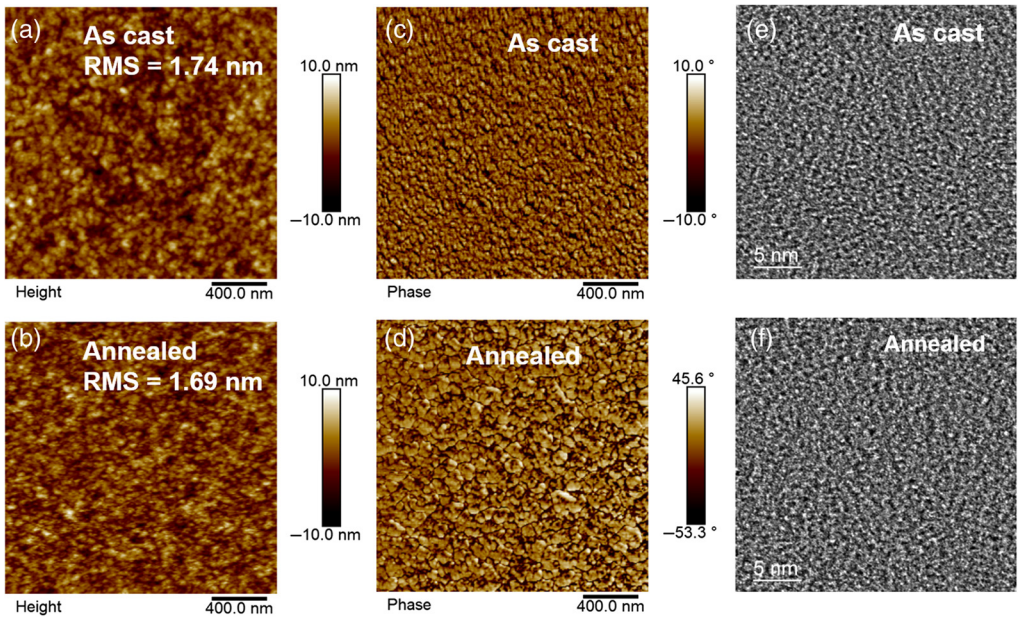

Fig. 4 (a) and (b) AFM height images, (c) and (d) phase images, and (e) and (f) TEM images of the as-cast and annealed PB3T:IEICO-4F blends films.

Table 2 The summary of different methods for estimation of bandgaps in typical D/A systems with E_{loss} below 0.7 eV in PSCs.

Active layer	Method 1[a] E_g/E_{loss} (eV)	Method 2[b] E_g/E_{loss} (eV)	Method 3[c] E_g/E_{loss} (eV)	Method 4[d] E_g/E_{loss} (eV)	References
PBQ-QF:IEICO-4F	—	—	—	1.36/0.62	14
PTB7-Th:$PC_{71}BM$	—	—	—	1.67/0.87	14
P3TEA:SF-PDI2	—	—	—	1.72/0.61	11
PM6:ITC-2Cl	—	—	—	1.58/0.67	34
PffBT4T-2DT:FBR	—	—	1.60/0.50	—	35
PTB7-Th:DTPC-IC	—	—	1.21/0.42	—	36
PTB7-Th:DTPC-DFIC	—	—	1.21/0.45	—	36
D-IDTT-SQ:$PC_{71}BM$	—	—	1.49/0.56	—	37
PvBDTTAZ:O-IDTBR	—	—	1.63/0.55	—	38
PDBT(E)BTz-p/IT-4F			1.53/0.55		39
PBDB-T: HF-PCIC:IEICO-4F	1.35/0.59	—	—	—	40
PB3T:IEICO-4F	1.33/0.52	1.32/0.50	1.28/0.46	1.34/0.52	This work

[a]Method 1 refers to the method using the derivatives of EQEs for determination of bandgap.
[b]Denotes the method using Tauc plot.
[c]Absorption edge was applied to determine the bandgap.
[d]Denotes the method of the crosspoint of absorption and emission spectra.

solar cells resulting from the radiative recombination above the bandgap based on the SQ limit theory, depends only on the bandgap as mentioned above. The second term ΔE_2 originates from additional radiative recombination below the bandgap (or CTS). This part cannot be ignored for PSCs because of the existence of the below bandgap CTS, which has lower emission luminescence efficiency than the pure donor and/or acceptor material. The energetic driving force in PSC is the energy offset of a singlet exciton and the energy of CTS ($E_X - E_{CT}$), which historically has

been considered to be at least 0.3 eV for efficient charge separation at the interface of D/A.[40,43] To get minimal ΔE_2, it is necessary to decrease the driving force, i.e., maximize E_{CT}. This, however, was thought to lead to less efficient charge separation in PSCs. It is exciting to see some exceptions in recent years with reduced tradeoff between decreased charge separation driving force and efficient PSCs,[11,35,36,44–48] mainly in mid bandgap NFA-based PSCs. Here, in this LBG NFA PSC system, we measured the EL spectra of the pure and blend film-based devices [see Fig. 4(a)]. The EL spectrum of the blend is very close to that of pure IEICO-4F device, exhibiting no emission from the CTS. In this case, we could get the safe conclusion that very close energy of E_X and E_{CT} (close zero driving force) and thus no sub-bandgap absorption in this blend. The weakly bound state at the interface of D/A is not the key contribution to E_{loss} in this case. We could indicate the energy offset driving force is near zero in this blend, which is much smaller than that for reported highly efficient PSCs. However, a decent EQE_{max} of ~40% was still obtained for this D/A system with such small driving force for charge separation.

In an ideal solar cell, the recombination mechanism only includes radiative recombination and thus can reach the maximum V_{OC} (V_{OC}^{rad}). In real cases, another important contribution to energy loss is assigned to ΔE_3 originating from nonradiative recombination. Given the negligible ΔE_2 and unavoidable ΔE_1, more efforts were put on ΔE_3 in our work. ΔE_3 can alternatively be calculated using the following equation: $q\Delta V_{OC}^{non\text{-}rad} = -kT\ \ln(EQE_{EL})$, as mentioned above,[12] where EQE_{EL} is the radiative quantum yield of EL measured by injection current in the dark. Therefore, maximizing the EQE_{EL} is considered to be a potential way to minimize $q\Delta V_{OC}^{non\text{-}rad}$ and thus get high V_{OC} for organic solar cells. For inorganic and perovskite solar cells, the $q\Delta V_{OC}^{non\text{-}rad}$ is about 0.18 to 0.25 eV,[12] whereas for fullerene-based PSCs, $q\Delta V_{OC}^{non\text{-}rad}$ is much larger, of about 0.38 to 0.44 eV, implying low yield EQE_{EL} on the order of magnitude 10^{-8} to 10^{-6}.[12] With the development of state-of-the-art nonfullerene-based PSCs, The $qV_{OC}^{non\text{-}rad}$ value is updated by applying suitable energy level blend systems as small as 0.21 eV with enhanced EQE_{EL} of 0.03%[14] using mid-bandgap NFA IT-M blended with PDCBT-2F. In our work, EL measurement was performed to determine $q\Delta V_{OC}^{non\text{-}rad}$ to be 0.20 eV for the best V_{OC} devices (as-cast film based device), showing remarkable emission efficiency of 0.051%, which is among the highest EL yield reported in efficient PSCs. The suppression of nonradiative recombination and thus high EQE_{EL} in this blend device attribute to low V_{OC} loss (Table 3).

It is noted that with the addition of more IEICO-4F, the EL spectra were observed with clear red-shift [Fig. 5(b)], which is consistent with the varied V_{OC} with the increase of D/A ratios in Table 1. Under different injected current density [Fig. 5(c)], the EL intensity of the blend film-based device increased with the higher current injection, however, no shift of the main peak position was observed with higher injected currents and there is no spectra shape change, indicating that the emission peak is from the same state. Since the EQE_{EL} values for the blend devices have slight dependence on the injected charge carrier density and not always constant, the EQE_{EL} of the blends before and after TA versus injected current density was plotted in Fig. 5(d). Clearly, the D/A blends without TA treatment exhibit larger EQE_{EL} than those with posttreatment, which correlates with the smaller energy losses shown in Table 1.

3 Conclusion

In summary, we have investigated a very low V_{OC} loss PSC system consisting of deep HOMO level wide-bandgap polymer donor and LBG NFA with very small driving force but with EQE_{max} close to 40% and the probability of charge dissociation over 80%. The EL spectra of the blend-film based devices exhibit almost the same shape as that of the pure acceptor, indicating negligible driving force for charge seperation for interfacial state at D/A and reduced radiative recombination below bandgap. The photovoltage loss ($E_{gap} - qV_{OC}$) as small as 0.46 eV is

Table 3 Summary of E_{loss} (in eV units) for PB3T:IEICO-4F-based as-cast devices.

Devices	E_{gap}[a]	qVOC	E_{loss}	$qV_{oc}^{rad,SQ}$	$qV_{oc}^{rad,below\ gap}$	ΔE_1	ΔE_2	ΔE_3
As-cast	1.32	0.82	0.50	1.06	1.02	0.26	0.04	0.20

[a]The optical bandgap used here is determined by Tauc plot.

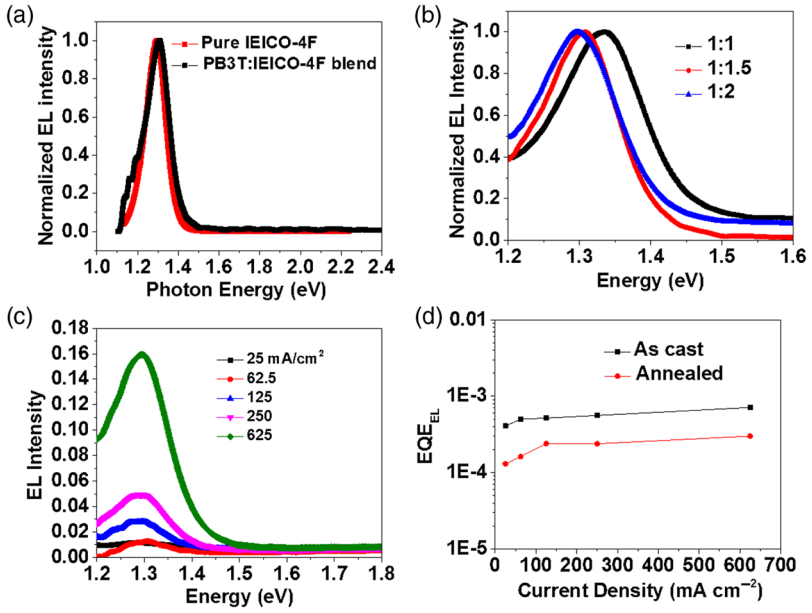

Fig. 5 (a) Normalized EL spectra of neat IEICO-4F and (b) Normalized emission intensity of PB3T:IEICO-4F devices at different D/A ratios. (c) The EL intensity of PB3T:IEICO-4F devices at different injection currents. (d) EQE_{EL} values of as-cast and annealed devices versus injected current densities.

reported, which is among the very few cases of EQE ~40% with E_{loss} <0.5 eV. This blend-film based devices with small driving force have exhibited high EQE_{EL} of 5.1×10^{-4}, leading to close to record low $\Delta V_{OC}^{non\text{-}rad}$ of 0.20 eV, which is comparable to inorganic and perovskite solar cells. Our work shows that a proper combination of deep HOMO wide-bandgap PB3T and LBG IEICO-4F can successfully reduce solar cell photovoltage energy losses to below 0.5 eV by decreasing driving force and the suppression of nonradiative recombination process. It is therefore proven the potential of PSCs toward higher performance.

4 Appendix A: Experimental Section

4.1 *Materials*

All reagents and solvents, unless otherwise specified, were purchased from J&K Scientific, Aldrich and Energy Chemical Ltd, and were used without further purification. IEICO-4F was purchased from Solarmer Materials, Inc. PB3T, and was synthesized according to the literature.

4.2 *Device Fabrication and Characterization*

Organic solar cells were fabricated on glass substrates commercially precoated with a layer of ITO in the conventional structure of ITO/PEDOT:PSS/active layer/PFN-Br/Ag. First, the glass/ITO substrates were cleaned using detergent, deionized water, acetone and isopropanol consecutively for every 30 min, and then treated in an ultraviolet ozone for 20 min. A thin layer (~30 nm) of PEDOT:PSS (Clevios 4083) was spin-coated onto precleaned substrates at 3000 rpm for 30 s and then annealed on hotplate at 150°C for 15 min. Then, the substrates were transferred to a glovebox. The active layer solution was spin coated from 10 mg/mL chlorobenzene solution for polymer concentration (D:A = 1:1.5) at 2500 rpm for 60 s to form an active layer of around 100 nm. Then TA was performed to optimize the device at various temperatures. Then, the cathode interlayer PFN-Br was spin coated at 3000 rpm for 30 s. At last, the Ag (90 nm) electrode was deposited by thermal evaporation with mask to complete the device with an active area of 0.08 cm^2.

The current density–voltage (J–V) curves of PSCs were measured with Keithley 236 measurement source units under 1 sun, AM 1.5G spectrum from a solar simulator (Enlitech, Taiwan),

and the light intensity was calibrated with a standard PV reference cell. The EQE spectra were measured with a QE-R3011 system from Enlitech.

5 Appendix B: Tables and Figures

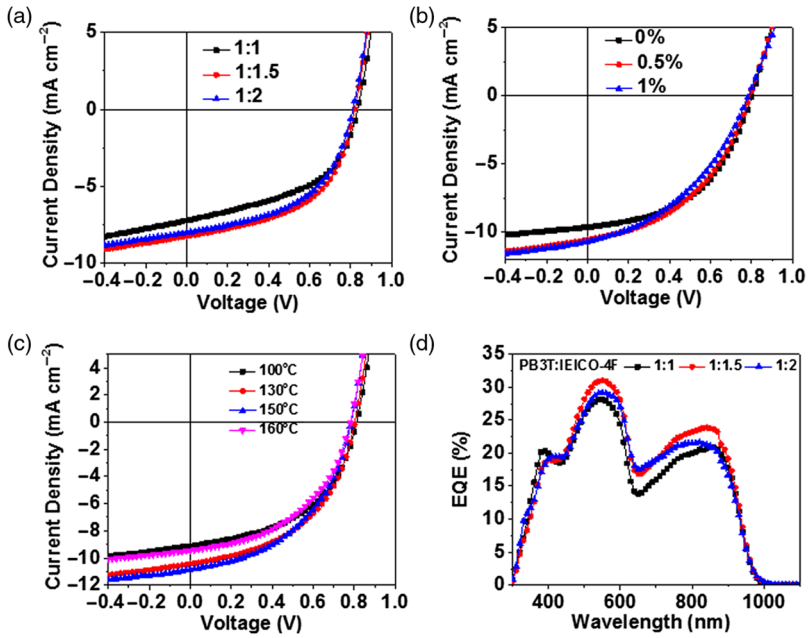

Fig. 6 The *J–V* curves of PB3T:IEICO-4F-based devices with different (a) D/A weight ratios, (b) volume amounts of DIO as additive, (c) TA temperatures, and (d) EQE spectra for PSC devices with different D/A ratios.

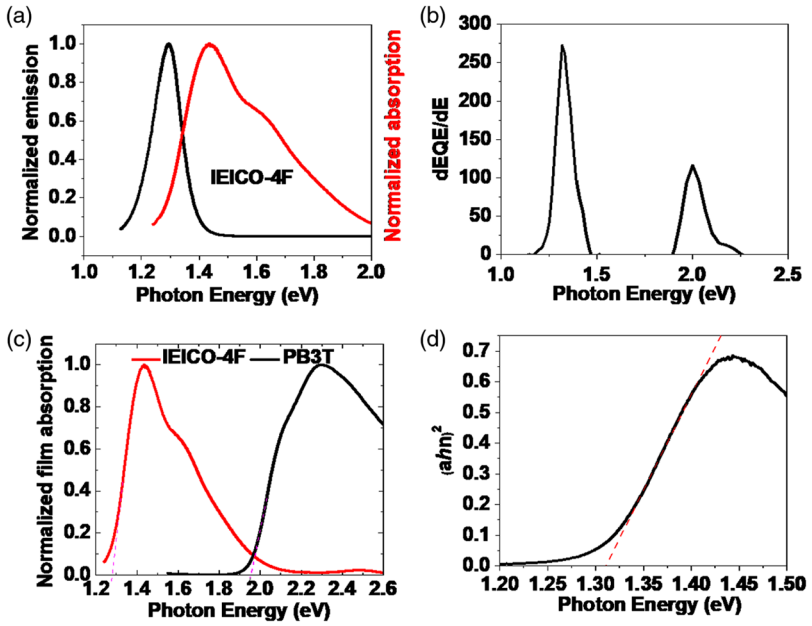

Fig. 7 Methods used for the determination of bandgap of IEICO-4F. (a) The optical bandgap (E_g^{opt}) of IEICO-4F (1.34 eV) was estimated from intersection of the normalized absorption and electroluminescence emission spectra. (b) Distributions of E_g^{opt} for PB3T:IEICO-4F blends using the derivatives of EQE curve (1.33 eV). (c) Optical bandgap estimation using absorption edge of lower bandgap component—IEICO-4F (1.28 eV). (d) Tauc plot was applied to measure E_g^{opt} of IEICO-4F (1.32 eV).

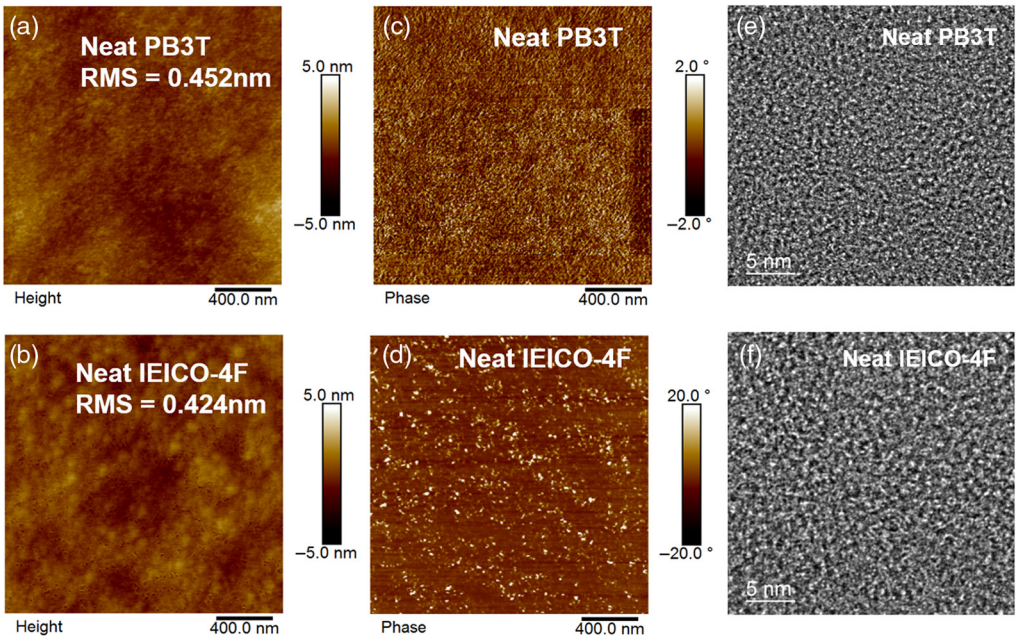

Fig. 8 (a) and (b) AFM height images, (c) and (d) phase images, and (e) and (f) TEM images of the neat PB3T and neat IEICO-4F films.

Table 4 Device performances with different D/A weight ratios.

D/A ratio	V_{OC} (V)	J_{SC} (mA/cm^2)	FF	PCE$_{avg}$ (%)	PCE$_{max}$ (%)	$\Delta V_{OC}^{non\text{-}rad}$ (V)
1:1	0.83	7.27	0.49	2.73	2.96	0.21
1:1.5	0.82	8.23	0.52	3.50	3.51	0.20
1:2	0.81	7.96	0.51	3.07	3.29	0.21

Note: The average PCEs were calculated from 10 independent cells.

Table 5 Device parameters of devices with different amounts of additive DIO at the same donor and acceptor weight ratio of 1:1.5

D/A	DIO (%)	V_{OC} (V)	J_{SC} (mA/cm^2)	FF	PCE$_{avg}$ (%)	PCE$_{max}$
PB3T:IEICO-4F (1:1.5, wt.%/wt.%)	0	0.80	9.59	0.49	3.71	3.76
	0.5	0.80	10.51	0.44	3.68	3.70
	1	0.78	10.63	0.41	3.32	3.40

Note: The average PCEs were calculated from 10 independent cells.

Table 6 Detailed performances of devices under different TA temperatures.

Active layer	Temperature (°C)	V_{OC} (V)	J_{SC} (mA/cm^2)	FF	PCE$_{avg}$ (%)	PCE$_{max}$ (%)
PB3T:IEICO-4F (1:1.5, wt.%/wt.%)	100	0.81	9.11	0.50	3.62	3.65
	130	0.80	10.44	0.48	4.00	4.06
	150	0.78	10.85	0.47	3.93	4.00
	160	0.78	9.46	0.47	3.29	3.48

Note: The average PCEs were calculated from 10 independent cells.

Table 7 Detailed performances under TA time optimization for devices at 130°C.

Active layer	Time (min)	V_{OC} (V)	J_{SC} (mA/cm^2)	FF	PCE_{avg} (%)	PCE_{max} (%)
PB3T:IEICO-4F (1:1.5 wt.%/wt.%)	0	0.81	8.59	0.50	3.28	3.48
	5	0.80	10.35	0.49	4.00	4.06
	10	0.79	11.20	0.47	4.14	4.16
	20	0.78	10.88	0.43	3.62	3.65

Note: The average PCEs were calculated from 10 independent cells.

Acknowledgments

G.L. thanks funding support from Shenzhen Science and Technology Innovation Commission (Project No. JCYJ20170413154602102), the Research Grants Council of Hong Kong (GRF grant 15218517), the Project of Strategic Importance provided by the Hong Kong Polytechnic University (ProjectCode: 1-ZE29), and the State Key Laboratory of Luminescent Materials and Devices, South China University of Technology.

References

1. G. Li, R. Zhu, and Y. Yang, "Polymer solar cells," *Nat. Photonics* **6**(3), 153–161 (2012).
2. B. Fan et al., "Fine-tuning of the chemical structure of photoactive materials for highly efficient organic photovoltaics," *Nat. Energy* **3**(12), 1051–1058 (2018).
3. J. Zhang et al., "Highly efficient semitransparent organic solar cells with color rendering index approaching 100," *Adv. Mater.* **31**(10), 1807159 (2019).
4. J. Yuan et al., "Single-junction organic solar cell with over 15% efficiency using fused-ring acceptor with electron-deficient core," *Joule* **3**(4), 1140–1151 (2019).
5. X. Xu et al., "Single-junction polymer solar cells with 16.35% efficiency enabled by a platinum(II) complexation strategy," *Adv. Mater.* **31**, 1901872 (2019).
6. Y. Cui et al., "Achieving over 15% efficiency in organic photovoltaic cells via copolymer design," *Adv. Mater.* **31**(14), 1808356 (2019).
7. G. Yu et al., "Polymer photovoltaic cells: enhanced efficiencies via a network of internal donor-acceptor heterojunctions," *Science* **270**(5243), 1789–1791 (1995).
8. S. M. Menke et al., "Understanding energy loss in organic solar cells: toward a new efficiency regime," *Joule* **2**(1), 25–35 (2018).
9. J. Hou et al., "Organic solar cells based on non-fullerene acceptors," *Nat. Mater.* **17**(2), 119–128 (2018).
10. U. Rau, "Reciprocity relation between photovoltaic quantum efficiency and electroluminescent emission of solar cells," *Phys. Rev. B* **76**(8), 085303 (2007).
11. J. Liu et al., "Fast charge separation in a non-fullerene organic solar cell with a small driving force," *Nat. Energy* **1**(7), 16089 (2016).
12. J. Yao et al., "Quantifying losses in open-circuit voltage in solution-processable solar cells," *Phys. Rev. Appl.* **4**(1), 014020 (2015).
13. W. Shockley and H. J. Queisser, "Detailed balance limit of efficiency of p-n junction solar cells," *J. Appl. Phys.* **32**(3), 510–519 (1961).
14. D. Qian et al., "Design rules for minimizing voltage losses in high-efficiency organic solar cells," *Nat. Mater.* **17**(8), 703–709 (2018).
15. H. Bin et al., "11.4% efficiency non-fullerene polymer solar cells with trialkylsilyl substituted 2D-conjugated polymer as donor," *Nat. Commun.* **7**, 13651 (2016).
16. H. Fu et al., "Suppression of recombination energy losses by decreasing the energetic offsets in perylene diimide-based nonfullerene organic solar cells," *ACS Energy Lett.* **3**(11), 2729–2735 (2018).

17. S. Chen et al., "Efficient nonfullerene organic solar cells with small driving forces for both hole and electron transfer," *Adv. Mater.* **30**(45), 1804215 (2018).
18. F. D. Eisner et al., "Hybridization of local exciton and charge-transfer states reduces nonradiative voltage losses in organic solar cells," *J. Am. Chem. Soc.* **141**(15), 6362–6374 (2019).
19. Z. He et al., "Single-junction polymer solar cells with high efficiency and photovoltage," *Nat. Photonics* **9**(3), 174–179 (2015).
20. H.-Y. Chen et al., "Polymer solar cells with enhanced open-circuit voltage and efficiency," *Nat. Photonics* **3**(11), 649–653 (2009).
21. D. Veldman, S. C. J. Meskers, and R. A. J. Janssen, "The energy of charge-transfer states in electron donor–acceptor blends: insight into the energy losses in organic solar cells," *Adv. Funct. Mater.* **19**(12), 1939–1948 (2009).
22. W. Li et al., "High quantum efficiencies in polymer solar cells at energy losses below 0.6 eV," *J. Am. Chem. Soc.* **137**(6), 2231–2234 (2015).
23. K. Gao et al., "Deep absorbing porphyrin small molecule for high-performance organic solar cells with very low energy losses," *J. Am. Chem. Soc.* **137**(23), 7282–7285 (2015).
24. K. Kawashima et al., "High-efficiency polymer solar cells with small photon energy loss," *Nat. Commun.* **6**, 10085 (2015).
25. L. Dou et al., "Tandem polymer solar cells featuring a spectrally matched low-bandgap polymer," *Nat. Photonics* **6**(3), 180–185 (2012).
26. Z. Xiao, X. Jia, and L. Ding, "Ternary organic solar cells offer 14% power conversion efficiency," *Sci. Bull.* **62**(23), 1562–1564 (2017).
27. Y. Lin et al., "A facile planar fused-ring electron acceptor for as-cast polymer solar cells with 8.71% efficiency," *J. Am. Chem. Soc.* **138**(9), 2973–2976 (2016).
28. S. Li et al., "Energy-level modulation of small-molecule electron acceptors to achieve over 12% efficiency in polymer solar cells," *Adv. Mater.* **28**(42), 9423–9429 (2016).
29. H. Yao et al., "Design, synthesis, and photovoltaic characterization of a small molecular acceptor with an ultra-narrow bandgap," *Angew. Chem. Int. Ed. Engl.* **56**(11), 3045–3049 (2017).
30. X. Song et al., "Controlling blend morphology for ultrahigh current density in nonfullerene acceptor-based organic solar cells," *ACS Energy Lett.* **3**(3), 669–676 (2018).
31. D. Liu et al., "Molecular design of a wide-band-gap conjugated polymer for efficient fullerene-free polymer solar cells," *Energy Environ. Sci.* **10**(2), 546–551 (2017).
32. W. Zhao et al., "Molecular optimization enables over 13% efficiency in organic solar cells," *J. Am. Chem. Soc.* **139**(21), 7148–7151 (2017).
33. S. R. Cowan, A. Roy, and A. J. Heeger, "Recombination in polymer-fullerene bulk heterojunction solar cells," *Phys. Rev. B* **82**(24), 245207 (2010).
34. Z. Luo et al., "Reduced energy loss enabled by a chlorinated thiophene-fused ending-group small molecular acceptor for efficient nonfullerene organic solar cells with 13.6% efficiency," *Adv. Energy Mater.* **9**(18), 1900041 (2019).
35. D. Baran et al., "Reduced voltage losses yield 10% efficient fullerene free organic solar cells with >1 V open circuit voltages," *Energy Environ. Sci.* **9**(12), 3783–3793 (2016).
36. Z. Yao et al., "Dithienopicenocarbazole-based acceptors for efficient organic solar cells with optoelectronic response over 1000 nm and an extremely low energy loss," *J. Am. Chem. Soc.* **140**(6), 2054–2057 (2018).
37. D. Yang et al., "Low-band-gap small molecule for efficient organic solar cells with a low energy loss below 0.6 eV and a high open-circuit voltage of over 0.9 V," *ACS Energy Lett.* **2**(9), 2021–2025 (2017).
38. S. Chen et al., "A wide-bandgap donor polymer for highly efficient non-fullerene organic solar cells with a small voltage loss," *J. Am. Chem. Soc.* **139**(18), 6298–6301 (2017).
39. D. Liu et al., "Design of wide-bandgap polymers with deeper ionization potential enables efficient ternary nonfullerene polymer solar cells with 13% efficiency," *J. Mater. Chem. A* **7**(23), 14153–14162 (2019).
40. L. Zhan et al., "A near-infrared photoactive morphology modifier leads to significant current improvement and energy loss mitigation for ternary organic solar cells," *Adv. Sci.* **5**(8), 1800755 (2018).

41. P. L. Qin et al., "Stable and efficient organo-metal halide hybrid perovskite solar cells via pi-conjugated Lewis base polymer induced trap passivation and charge extraction," *Adv. Mater.* **30**(12), 1706126 (2018).
42. M. C. Scharber et al., "Design rules for donors in bulk-heterojunction solar cells towards 10% energy-conversion efficiency," *Adv. Mater.* **18**(6), 789–794 (2006).
43. G. Li, W.-H. Chang, and Y. Yang, "Low-bandgap conjugated polymers enabling solution-processable tandem solar cells," *Nat. Rev. Mater.* **2**(8), 17043 (2017).
44. R. A. Janssen and J. Nelson, "Factors limiting device efficiency in organic photovoltaics," *Adv. Mater.* **25**(13), 1847–1858 (2013).
45. J. Yuan et al., "Enabling low voltage losses and high photocurrent in fullerene-free organic photovoltaics," *Nat. Commun.* **10**(1), 570 (2019).
46. W. Gao et al., "Simultaneously increasing open-circuit voltage and short-circuit current to minimize energy loss of organic solar cells via designing asymmetrical non-fullerene acceptor," *J. Mater. Chem. A* **7**(18), 11053–11061 (2019).
47. X. Gong et al., "Bulk heterojunction solar cells with large open-circuit voltage: electron transfer with small donor-acceptor energy offset," *Adv. Mater.* **23**(20), 2272–2277 (2011).
48. S. D. Dimitrov et al., "On the energetic dependence of charge separation in low-band-gap polymer/fullerene blends," *J. Am. Chem. Soc.* **134**(44), 18189–18192 (2012).

Biographies of the authors are not available.